ANSWERS TO SELECTED PROBLEMS

Exercises for Chapter 1

(1) We start with the relation

$$\Delta\nu \propto \sqrt{\rho},$$

which, if we use the Sun as a standard results in

$$\frac{\Delta\nu}{\Delta\nu_\odot} = \sqrt{\frac{\rho}{\rho_\odot}},$$

or in other words

$$\rho = \rho_\odot \left(\frac{\Delta\nu}{\Delta\nu_\odot}\right)^2.$$

Assuming that the solar density is 1.408 g cm^{-3}, we derive the density of the given stars to be:

(a) 1.177 g cm^{-3}
(b) 1.113 g cm^{-3}
(c) 0.504 g cm^{-3}
(d) 0.240 g cm^{-3}
(e) 0.067 g cm^{-3}
(f) 0.011 g cm^{-3}
(g) 0.007 g cm^{-3}

Density alone is not a very good indicator of evolutionary state, however, it is enough to separate dwarfs from giants. Stars (a), (b) and (c) are dwarfs, and stars (f) and (g) are giants. Without a knowledge of temperature (or without individual mode frequencies), the evolutionary state of stars (d) and (e) are difficult to judge. They could be subgiants.

(2) The scaling relations tell us that

$$\left(\frac{\Delta\nu}{\Delta\nu_\odot}\right)^2 = \frac{M/M_\odot}{(R/R_\odot)^3}, \tag{1}$$

and

$$\frac{\nu_{\rm max}}{\nu_{\rm max,\odot}} = \frac{M/M_\odot}{(R/R_\odot)^2}\sqrt{\frac{T_{\rm eff}}{T_{\rm eff,\odot}}}. \tag{2}$$

On diving Eq. (2) by Eq. (1) and rearranging the terms we get

$$\frac{R}{R_\odot} = \left(\frac{\nu_{\rm max}}{\nu_{\rm max,\odot}}\right)\left(\frac{\Delta\nu}{\Delta\nu_\odot}\right)^{-2}\left(\frac{T_{\rm eff}}{T_{\rm eff,\odot}}\right)^{1/2}. \tag{3}$$

Substituting $R/R_\odot$ from Eq. (3) into Eq. (2) gives us

$$\frac{M}{M_\odot} == \left(\frac{\nu_{\rm max}}{\nu_{\rm max,\odot}}\right)^3\left(\frac{\Delta\nu}{\Delta\nu_\odot}\right)^{-4}\left(\frac{T_{\rm eff}}{T_{\rm eff,\odot}}\right)^{3/2}. \tag{4}$$

Eqs. (3) and (4) are the required results.

(4) The evolutionary state of a star can be gauged by the number of avoided crossing, i.e., mixed modes, seen in the échelle diagram of the star. The classification of the stars is as follows:

KIC04448777: Red giant, with $\Delta\nu \approx 17$ μHz
KIC05955122: Subgiant with $\Delta\nu \approx 49.5$ μHz
KIC10273246: Subgiant with $\Delta\nu \approx 48.7$ μHz
KIC10920273: Subgiant with $\Delta\nu \approx 57.2$ μHz
KIC11395018: Subgiant with $\Delta\nu \approx 47.85$ μHz
KIC11772920: Main-sequence stars with $\Delta\nu \approx 157.3$ μHz
KIC12069127: Main-sequence stars with $\Delta\nu \approx 47.8$ μHz
KIC12069449: Main-sequence stars with $\Delta\nu \approx 117.5$ μHz
KIC12258514: Main-sequence stars with $\Delta\nu \approx 74.85$ μHz

Exercises for Chapter 2

(1)(a) Since $\rho = \rho_c$ at $r = 0$ and $\rho = 0$ at $r = R$, it follows that

$$\rho = \rho_c(1 - r/R) = \rho_c(1 - x), \tag{1}$$

where $x = r/R$. Mass within any radius r is given by

$$m(r) = \int_0^r 4\pi r^2 \rho(r) \mathrm{d}r = \frac{4\pi}{3}\rho_c r^3 \left(1 - \frac{3}{4}\right). \tag{2}$$

From Eq. (2) we see that

$$m(R) = M = \frac{\pi}{3}\rho_c R^3, \tag{3}$$

thus

$$m(r) = M(4x^3 - 3x^4). \tag{4}$$

(1)(b) From Problem (1)(a), Eq. (3) it follows that

$$\rho_c = \frac{3}{\pi}\frac{M}{R^3}. \tag{5}$$

(1)(c) We start evaluating P using $\mathrm{d}P/\mathrm{d}r = -g\rho$, using the boundary conditions $P - P_c$ at $r = 0$ and $P = 0$ at $r = 1$. Thus

$$P = P_c - \int_0^r \frac{Gm(r)\rho(r)}{r^2}\mathrm{d}r. \tag{5}$$

Applying the condition $P = 0$ at $r = R$ in Eq. (5) gives

$$P_c = \frac{5}{4\pi}GM^2R^4, \tag{6}$$

which on substituting in Eq. (5) gives the required result.

(1)(d) From the ideal gas law we get

$$T = \frac{\mu}{\mathcal{R}}\frac{P}{\rho}.$$

Substituting for ρ and P, we get

$$T = \frac{\mu}{\mathcal{R}}\frac{GM}{12R}\left(9x^3 - 19x^2 + 5x + 5\right). \tag{7}$$

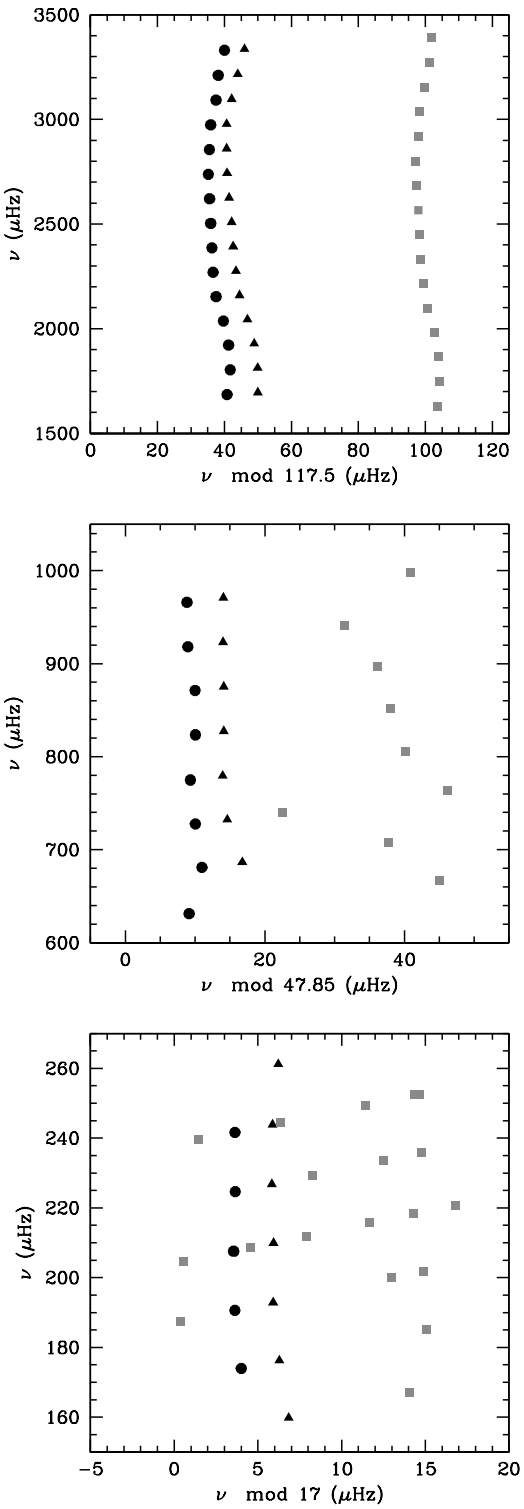

Figure 1: Top to bottom: The échelle diagrams of KIC12069449, KIC11395018 and KIC04448777. Triangles are $l = 0$ modes, squares are $l = 1$ modes and circles $l = 2$ modes

(1)(e) We are given that

$$\epsilon = \epsilon_0 \rho^k \left(\frac{T}{T_0}\right)^n = \epsilon_0 \rho_c^k \left[\left(\frac{\mu}{\mathcal{R}}\right)\frac{GM}{12RT_0}\right]^n (1-x)^k (9x^3 - 19x^2 + 5x + 5)^n. \tag{8}$$

Thus

$$L = 4\pi R^3 \epsilon_0 \rho_c^{k+1} \left[\left(\frac{\mu}{\mathcal{R}}\right)\frac{GM}{12RT_0}\right]^n \int_0^x x^2 (1-x)^{k+1} (9x^3 - 19x^2 + 5x + 5)^n \mathrm{d}x.$$

But $9x^3 - 19x^2 + 5x + 5 = (1-x)(5 + 10x - 9x^2)$ which means that luminosity may be expressed as

$$L = L_0 \int_0^1 x^2 (1-x)^{k+n+1} (5 + 10x - 9x^2)^n \mathrm{d}x.$$

For $k = 1, n = 4$ the integral is

$$625x^3)/3 + (625x^4)/2 - 2025x^5 - 1250x^6 + (77025x^7)/7 - (20025x^8)/4 - (83735x^9)/3 + 42972x^{10} + (14571x^{11})/11 - (392033x^{12})/6 + (1084465x^{13})/13 - (380070x^{14})/7 + 20493x^{15} - (34263x^{16})/8 + (6561x^{17})/17$$

(2)(a) We use

$R_\odot = 6.96 \times 10^{10}$ cm

$M_\odot = 1.989 \times 10^{33}$ g

$G = 6.67 \times 10^{-8}$ cm^3 g^{-1} s^{-2}

Thus we find that

$$\rho_c = \frac{3}{\pi}\frac{M_\odot}{R_\odot^3} = 5.63 \text{g cm}^3, \tag{1}$$

and

$$P_c = \frac{5}{4\pi}\frac{GM_\odot^2}{R_\odot^4} = 4.47 \times 10^{15} \text{ dyne cm}^{-2}. \tag{2}$$

Note that modern solar models that agree well with helioseismic results have $\rho_c \sim 154$ g cm^{-3}, and $P_c \sim 2.4 \times 10^{17}$dyne cm^{-2}.

(2)(b) We are given that $X = 0.74$, $Z = 0.02$ which means $Y = 0.24$. And we are asked to assume that the 'Sun' is chemically homogeneous. Thus the mean molecular weight μ in the core is approximately 0.6. The gas constant in cgs units is $\mathcal{R} = 8.31 \times 10^7$ ergs K^{-1} g^{-1}. Thus

$$P_c = \frac{\mu}{\mathcal{R}}\frac{P_c}{\rho_c} = 5.73 \times 10^6 \text{K}.$$

Modern solar models have $T_c \sim 1.5 \times 10^7$K.

(3) The difference between the two models is whether or not diffusion and gravitational settling of helium has been included. SolarModel1.txt lists the data for the model with diffusion and gravitational settling SolarModel2.txt is for the model without.

The inference about the settling can be inferred from the surface abundance of hydrogen and heavy elements. In Model 2, the abundances remain constant. For Model 1, the surface value of Z decreases due to settling, while the surface X increases (since $X+Y+Z = 1$). From X_{sure} and Z_{sure} one can calculate Y_{sure} to show that Y_{sure} decrease with age in Model 1 but remains constant in Model 2. One can also see that the metallicity in the core keeps increasing in Model 1, but is a constant in Model 2. Since these are main-sequence models, the Z in the core cannot increase because of nuclear reactions.

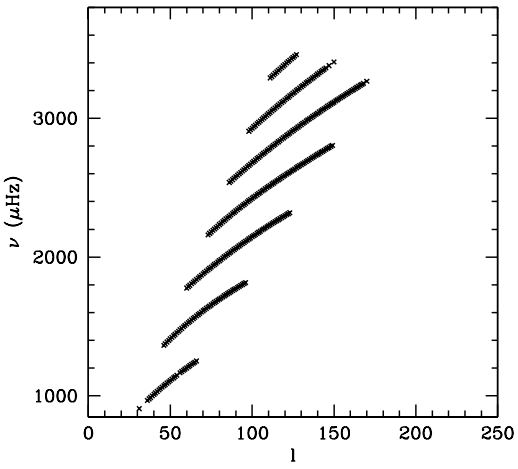

Figure 2: l-ν diagram of modes in `SolarFreq_MDI.txt` that have lower turning points between 0.9 and 0.95 $R_\odot$.

The convection-zone Y and Z of a star are always uniform because of fast mixing by convective eddies; diffusion causes Helium and heavy elements to accumulate at the convection-zone base. The increase in metallicity increases opacity, and as a result, models with diffusion have deeper convection zone (since opacity is larger at a higher temperature, $\nabla_{\rm rad}$ exceed $\nabla_{\rm ad}$ in layers with higher temperature, which in a star means a deeper layer). While the convection zone deepens in both models, the rate of change in Model 1 is higher because of the increasing metallicity at the base.

Exercises for Chapter 3

(1)(b) Yes, in stars 2 and 3.

(2) α needs to be about 1.5 to get a good curve. Even better results are obtained is α is allowed to be a function of frequency.

(3)(b) For the given solar frequencies and sound speed, one finds that modes with $20 \leq 0 \leq 30$ have lower turning points between about 0.36 and 0.87 $R_\odot$. Thus the maximum depth that we can probe with these modes is 0.36 $R_\odot$.

(3)(c) See Fig. 2 for the $l - \nu$ range of the modes that have lower turning points between 0.9 and $0.95R_\odot$.

(4)(a) See Fig. 3(a).

(4)(b) See Fig. 3(b).

(4)(c) As the peak is shifted from large r to smaller r, the frequency differences, when plotted as a function of frequencies become more oscillatory.

Exercises for Chapter 4

(1) We start from the general expression for photometric observations:

$$S_l = 2\sqrt{2l+1} \int_0^{\pi/2} P_l(\cos\theta) W(\cos\theta) \cos\theta \sin\theta \mathrm{d}\theta.$$

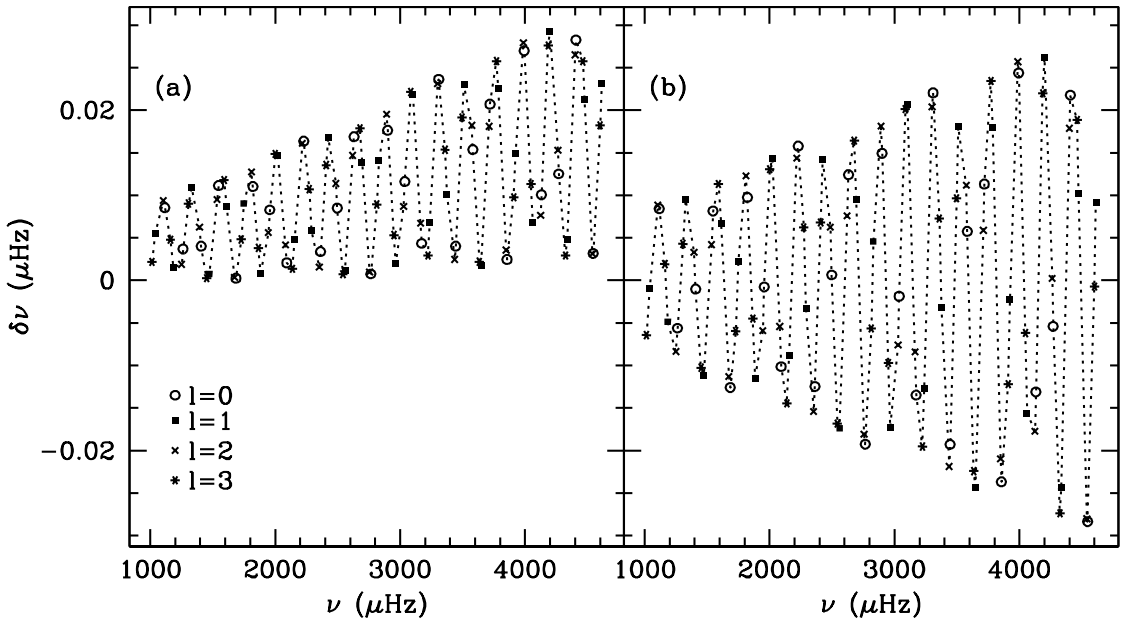

Figure 3: Answer to Problem 4(a) and 4(b) of Chapter 3. The points have been joined by a line to guide the eye.

With only one coefficient, the limb-darkening law takes the form

$$W(\cos\theta) = a + b\cos\theta,$$

with (cf. Eq. 4.2) $a \equiv 1 - c_1 = 2/5$, and $b \equiv c_1 = 3/5$.

Also, at $l = 1$, we have

$$P_l(\cos\theta) = \cos\theta.$$

We therefore write:

$$S_1 = 2\sqrt{3}\int_0^{\pi/2} \cos^2\theta(a + b\cos\theta)\sin\theta \mathrm{d}\theta.$$

We make the substitution $x = \cos\theta$, so that $\mathrm{d}x = -\sin\theta\mathrm{d}\theta$. The limits change to 0 (upper limit) and -1 (lower limit). This gives:

$$S_1 = -2\sqrt{3}\int_1^0 x^2(a + bx)\mathrm{dx},$$

$$S_1 = 2\sqrt{3}\int_0^1 (ax^2 + bx^3)\mathrm{dx}.$$

It then follows that:

$$S_1 = 2\sqrt{3}\left[\frac{ax^3}{3} + \frac{bx^4}{4}\right]_0^1 = 2\sqrt{3}\left[\frac{2}{15} + \frac{3}{20}\right].$$

Now, we also need to calculate the visibility for $l = 0$, which is:

$$S_0 = 2\int_0^{\pi/2} \cos\theta(a + b\cos\theta)\sin\theta \mathrm{d}\theta.$$

This becomes:

$$S_0 = 2\int_0^1 (ax + bx^2)\mathrm{dx},$$

giving:

$$S_0 = 2\left[\frac{ax^2}{2} + \frac{bx^3}{3}\right]_0^1 = 2\left[\frac{2}{10} + \frac{3}{15}\right].$$

The ratio is therefore:

$$(S_0/S_1)^2 = (1.23)^2 \simeq 1.51$$

(2) We start once more from the general expression for photometric observations:

$$S_l = 2\sqrt{2l+1}\int_0^{\pi/2} P_l(\cos\theta)W(\cos\theta)\cos\theta\sin\theta\mathrm{d}\theta.$$

Ignoring limb darkening, we have $W(\cos\theta) = 1$. At l=3, we have

$$P_3(\cos\theta) = 1/2(5\cos^3\theta - 3\cos\theta).$$

We therefore write:

$$S_3 = \sqrt{3}\int_0^{\pi/2} (5\cos^3\theta - 3\cos\theta)\cos\theta\sin\theta\mathrm{d}\theta.$$

We make the same substitutions as in the first problem. This gives:

$$S_3 = \sqrt{3}\int_0^1 (5x^4 - 3x^2)\mathrm{dx},$$

so that:

$$S_3 = \sqrt{3}\left[x^5 - x^3\right]_0^1 = 0.$$

The visibility is zero! It is only when we include limb-darkening, to give a non-uniform intensity over the disc, that the $l = 3$ modes have non-zero visibility.

(3) We start from:

$$L \propto R^2T^4$$

The amplitude of the oscillations in luminosity (the bolometric amplitude) is therefore given by:

$$\delta L/L = 2\delta R/R + 4\delta T/T$$

Guided by the question, we neglect the contribution from changes in radius, implying:

$$\delta L/L = 4\delta T/T.$$

The relevant temperature is close to the effective temperature of 5777 K. So, putting in the numbers, we have an implied change of just 5 milli-K.

To convert to narrow-band amplitudes, we use:

$$\left(\frac{\delta F_{\rm bol}}{F_{\rm bol}}\right) \simeq \left(\frac{\lambda}{623\,\mathrm{nm}}\right)\left(\frac{T_{\rm eff}}{5777\,\mathrm{K}}\right)\left(\frac{\delta F_\lambda}{F_\lambda}\right).$$

The value of 3.5 ppm corresponds to the bolometric amplitude. So we just need to substitute and re-arrange the above, to give the sought-for narrow=band amplitudes. They are 4.4 ppm (500 nm) and 2.7 ppm (800nm).

(4) The results depend upon whether or not the Mach-number dependence is included in the scaling relations for the granulation parameters.

We begin by using Eq. 4.41 to compute the maximum radial p-mode amplitudes, v, of both stars in Doppler velocity, using the data on $L \propto R^2 T_{\rm eff}^4$ and M provided in the question, and scaling by the given solar value. For the main-sequence star we obtain $v_1 \simeq 21\,{\rm cm\,s^{-1}}$, and for the evolved star we obtain $v_1 \simeq 65\,{\rm cm\,s^{-1}}$.

Next, to compute the corresponding bolometric amplitudes, $(\delta F_{\rm bol}/F_{\rm bol})$, we use Eq. 4.53 to scale from Doppler velocity to intensity but with the exponent in $T_{\rm eff}$ adjusted from 0.5 to unity (note the comment in the text below the equation). This gives $(\delta F_{\rm bol}/F_{\rm bol})_1 \simeq 3.9\,{\rm ppm}$ and $(\delta F_{\rm bol}/F_{\rm bol})_2 \simeq 15.7\,{\rm ppm}$.

The granulation amplitudes in intensity follow from Eq. 4.58. We have that $\sigma_{{\rm c},I,1} \simeq 46\,{\rm ppm}$ and $\sigma_{{\rm c},I,2} \simeq 128\,{\rm ppm}$ We then use Eq. 4.86 to convert the granulation amplitudes from intensity to Doppler velocity. Using the simpler scaling, which neglects the dependence on the Mach number, we obtain $\sigma_{{\rm c},v,1} \simeq 48\,{\rm cm\,s^{-1}}$ and $\sigma_{{\rm c},v,2} \simeq 117\,{\rm cm\,s^{-1}}$. With the Mach-number dependence included, we have $\sigma_{{\rm c},v,1} \simeq 67\,{\rm cm\,s^{-1}}$ and $\sigma_{{\rm c},v,2} \simeq 124\,{\rm cm\,s^{-1}}$.

Putting this all together, we find oscillation-to-granulation ratios of:

- 0.08 for star 1 and 0.12 for star 2, for observations in bolometric intensity;
- 0.44 for star 1 and 0.56 for star 2, for observations in Doppler velocity, and no dependence of the scalings on the Mach number; and
- 0.31 for star 1 and 0.52 for star 2, for observations in Doppler velocity, with the dependence on the Mach number included.

The choice of scaling does have some effect on the ratios in Doppler velocity – most notably for the less evolved star. The most striking aspect of the results is, however, that the ratio stays much lower in intensity than in Doppler velocity.

(5) To compute the granulation amplitude in Doppler velocity, $\sigma_{{\rm c},v}$, we use the same procedures as those outlined in the question above. We do so for scalings with and without the Mach-number dependence. Figure 4 shows the estimated velocities as a function of stellar age, t. Results without the Mach-number dependence follow the dotted line, while those with follow the dashed line.

To estimate the activity signal, $\sigma_{{\rm act},v}$, we use Eq. 4.88. First, we took values of $(\delta I/I) \simeq 0.45$ and $(\delta a/a) \simeq 0.3\,\%$ (see Section 4.3.2, which gives ranges of suitable values). To estimate the surface rotation period, we use the $t^{1/2}$ dependence and scale against the solar value of $\simeq 25\,{\rm days}$, i.e.,

$$P_{\rm rot} \simeq 25\,(t/4.6)^{1/2}\,,$$

with ages t in Gyr, suitably scaled to the solar age of 4.6 Gyr. We may then convert to the required $v \sin i$ using:

$$v \sin i \equiv \left(\frac{2\pi R}{P_{\rm rot}}\right) \sin i,$$

where R is the stellar radius. For our calculations we assume the star is viewed edge-on, so that $v \sin i = 1$. The solid line in Figure 4 shows the predicted $\sigma_{{\rm act},v}$.

Exercises for Chapter 5

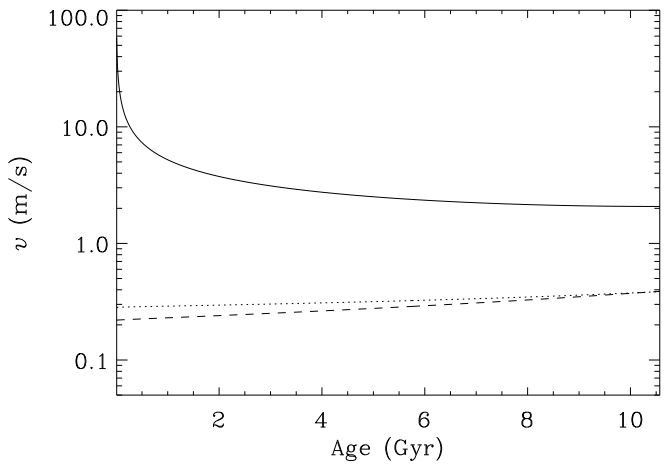

Figure 4: Solid line: predicted activity amplitude in Doppler velocity, $\sigma_{\mathrm{act},v}$. Dotted and dashed lines show predicted granulation amplitude in Doppler velocity, $\sigma_{\mathrm{c},v}$, with and without the dependence on Mach number.

(1) We start from Eq. 5.79, i.e.,

$$P_{\mathrm{tot}} \propto H_{\mathrm{env}} \Gamma_{\mathrm{env}}.$$

Next, Eq. 5.91 gives the dependence of the oscillation power envelope width on ν_{max}, i.e., $\Gamma_{\mathrm{env}}^{k}$, where for Sun-like stars we have $k \approx 1$.

To get the dependence of H_{env} on ν_{max} and T_{eff} we must go through several steps. First, Eq. 5.76 gives

$$H_{\mathrm{env}} \propto A_{\mathrm{max}}^{2}/\Delta\nu.$$

Next, from Eq. 5.87 we have:

$$A_{\mathrm{max}} \propto \nu_{\mathrm{max}}^{-s} T_{\mathrm{eff}}^{3.5s-r+1-\beta_{\mathrm{bol}}}.$$

where for *Kepler* observations $\beta_{\mathrm{bol}} = 0.8$. Finally, we need:

$$\Delta\nu \propto \nu_{\mathrm{max}}^{\beta},$$

where we take the value $\beta \simeq 0.77$. Putting this all together, we have:

$$H_{\mathrm{env}} \propto \nu_{\mathrm{max}}^{-2s} T_{\mathrm{eff}}^{7s-2r+2-2\beta_{\mathrm{bol}}},$$

and so:

$$P_{\mathrm{tot}} \propto \nu_{\mathrm{max}}^{-2s-\beta+k}\, T_{\mathrm{eff}}^{7s-2r+2-2\beta_{\mathrm{bol}}}.$$

We also adopt $k \simeq 1$, $s \simeq 0.7$ and $r \simeq 3.5$, from which we then get the required relation:

$$P_{\mathrm{tot}} \propto \nu_{\mathrm{max}}^{-1.2} T_{\mathrm{eff}}^{-1.7}.$$

(2) We begin by recalling that for main-sequence stars the width of the oscillation envelope is assumed to follow the scaling $\Gamma_{\mathrm{env}} = \nu_{\mathrm{max}}/2$ (Eq. 5.91). We then assume that the frequency range $\pm\nu_{\mathrm{max}}/2$ about ν_{max} will capture most of the observed power. The total power due to the flat shot-noise component is then equal to its power spectral density, i.e., $2\sigma^2\Delta t$, multiplied by the range ν_{max}.

To estimate the contribution from the granulation, we start from Eq. 5.99, i.e.,

$$P_{\mathrm{c}}(\nu) = \frac{b_{\mathrm{c}}}{1 + (2\pi\nu\tau_{\mathrm{c}})^{\beta_{\mathrm{c}}}}.$$

To progress to the approximate final expression provided in the answer, we make two assumptions. First, we assume that in the frequency vicinity of the mode spectrum, $(2\pi\nu\tau_{\rm c})^{\beta_{\rm c}} \gg 1$. We may then write the above as:

$$P_{\rm c}(\nu) \approx \frac{b_{\rm c}}{(2\pi\nu\tau_{\rm c})^{\beta_{\rm c}}}.$$

Second, we assume we may approximate the required area under the limit spectrum of the granulation as the power spectral density at $\nu_{\rm max}$, i.e.,

$$P_{\rm c}(\nu_{\rm max}) \approx \frac{b_{\rm c}}{(2\pi\nu_{\rm max}\tau_{\rm c})^{\beta_{\rm c}}},$$

multiplied by the range $\nu_{\rm max}$. This gives the granulation contribution

$$\nu_{\rm max}^{(1-\beta_{\rm c})}\left(\frac{b_{\rm c}}{(2\pi\tau_{\rm c})^{\beta_{\rm c}}}\right),$$

from which it then follows that:

$$B_{\rm tot} \approx 2\nu_{\rm max}\sigma^2\Delta t + \nu_{\rm max}^{(1-\beta_{\rm c})}\left(\frac{b_{\rm c}}{(2\pi\tau_{\rm c})^{\beta_{\rm c}}}\right).$$

(3) There are various ways one could approach calculating the results needed for this question. To compute the global SNR in the oscillations spectrum we use the following steps:

- We use Eqs. 5.76 and 5.79 to compute the solar value for the total detected power in the oscillations spectrum, $P_{\rm tot}$, which is $\simeq 231\,{\rm ppm}^2$. We then use Eq. 5.92 to compute $P_{\rm tot}$ along the evolutionary track, using the coefficients $t = -1.2$ and $u = -1.7$.
- We use the equation in the question above for the total background power, $B_{\rm tot}$. The shot-noise per cadence was estimated using (see also Eq. 6.49):

  $$\sigma({\rm Kp}) = 70\ \times 10^{\,[({\rm Kp}-9)/5]}\,{\rm ppm},$$

  where 70 ppm is the shot noise at Kp = 9. We estimated the granulation noise using Eq. 4.58 (scaled by the solar value given in the question). We also needed the granulation timescale, and for that we used Eq. 4.63, scaled to the solar value of 200 sec in the text.

The resulting SNR predictions are shown in Figure 5, for *Kepler* apparent magnitudes of Kp = 8 (solid line), Kp = 10 (dotted line) and Kp = 12 (dashed line). Predictions with and without the Mach-number dependence give very similar results, and so here we show those for the simpler predictions without the dependence. Note the low numbers associated with the global values.

(4) We begin by computing the respective $\nu_{\rm max}$ values for both stars, obtaining $\nu_{\rm max,1} = 459\,\mu$Hz for star 1 and $\nu_{\rm max,1} = 233\,\mu$Hz for star 2. Notice already that the frequency for star 1 lies well above the *Kepler* long-cadence (LC) Nyquist frequency (of $\simeq 283\,\mu$Hz).

Next, we have $A_1 \simeq 13.4\,$ppm and $A_2 \simeq 21.8\,$ppm. With estimates of the average large frequency separations also in hand, courtesy of the $\Delta\nu$ scaling relation ($\Delta\nu_1 \simeq 29.6\,\mu$Hz and $\Delta\nu_2 \simeq 17.7\,\mu$Hz), we may then use Eq. 5.76 to estimate the heights of the respective oscillation envelopes. We obtain $H_{\rm env,1} \simeq 9.4\,{\rm ppm}^2\,\mu{\rm Hz}^{-1}$ and $H_{\rm env,2} \simeq 41.6\,{\rm ppm}^2\,\mu{\rm Hz}^{-1}$.

We must also not forget to take into account the impact of signal attenuation due to the sampling of the data. For observations made in short cadence (SC), the respective $\nu_{\rm max}$ lie sufficiently far below the Nyquist frequency that the attenuation will be negligible. However, this is certainly not the case for LC data. Using Eq. 5.9, we obtain multiplicative attenuation factors in power of $\eta^2 \simeq 0.05$ for star 1 and $\eta^2 \simeq 0.55$ for star 2.

So, the height-to-background ratios we obtain are:

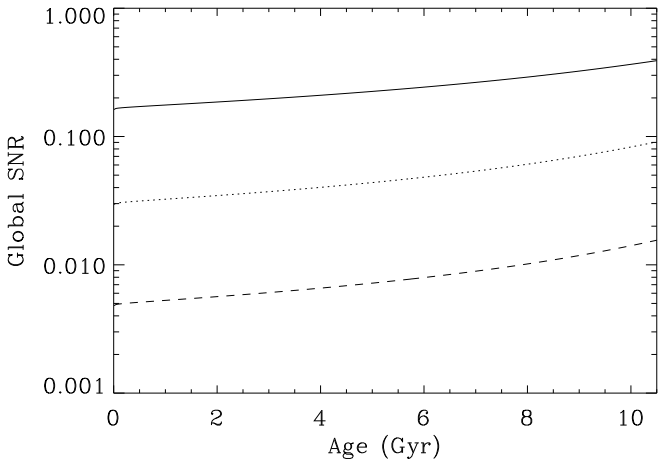

Figure 5: Predicted global SNR in the oscillation spectrum, for *Kepler* apparent magnitudes of Kp = 8 (solid line), Kp = 10 (dotted line) and Kp = 12 (dashed line).

– in short cadence, $9.4/300 \simeq 0.03$ for star 1; and $41.6/300 \simeq 0.14$ for star 2; and

– in long cadence, $0.05 \times 9.4/300 \simeq 0.0015$ for star 1; and $0.55 \times 41.6/300 \simeq 0.08$ for star 2.

The attenuation in LC clearly has a very pronounced effect on the predicted height-to-background ratio for star 1. The $\nu_{\rm max}$ of this star lies above the LC Nyquist frequency, $\nu_{\rm Nyq}$, and so for LC data the oscillation spectrum would be aliased down below the Nyquist, to a frequency centered on $\nu_{\rm Nyq} - (\nu_{\rm max} - \nu_{\rm Nyq}) \equiv 2\nu_{\rm Nyq} - \nu_{\rm max} \simeq 107\,\mu$Hz. Because the background power is shot-noise dominated, the background power spectral density below and above the Nyquist will be the same. However, had granulation noise been the dominant background term, we would have needed to have used the sub-Nyquist granulation to compute the height-to-background (and, strictly speaking, to have also worried about the granulation contribution in the super-Nyquist regime, which is aliased back down below the Nyquist, like the oscillations spectrum).

Even though $\nu_{\rm max}$ of star 2 lies $\approx 50\,\mu$Hz below the LC Nyquist frequency, the attenuation in LC does affect the observed height-to-background ratio, by a factor of around 2.

Exercises for Chapter 7

(2)(b) The properties of the "stars" are listed in Table . The value of $\nu_{\rm max}$ can be calculated from the listed data using the scaling relation.

Star No.	Mass $M_\odot$	Rad. $R_\odot$	Age Gyr	T_{eff} K	[Fe/H] dex	$\Delta\nu$
1	0.82	0.76	4.20	5534	−0.51	185.86
2	0.96	0.83	0.28	5015	0.29	175.53
3	0.82	0.84	11.80	5416	−0.34	158.09
4	1.14	1.02	0.19	6071	−0.06	139.80
5	1.00	1.00	6.13	5697	−0.07	134.66
6	1.16	1.08	0.41	6420	−0.31	129.22
7	1.68	1.46	0.24	8239	−0.19	99.49
8	1.18	1.39	3.90	6303	−0.38	89.20
9	1.04	1.37	9.14	5834	−0.16	86.28
10	1.20	1.58	3.65	6534	−0.52	74.60
11	1.18	1.73	7.01	5780	0.03	64.65
12	1.68	2.88	1.50	7361	−0.46	35.81
13	1.14	5.86	6.13	4926	−0.39	10.17
14	1.20	8.53	7.76	4533	0.10	5.93
15	2.46	14.28	0.71	5087	−0.45	3.92

Exercises for Chapter 8

(1) The true properties of the models can be found in the paper Reese et al. (2016), A&A (arXiv:1604.08404) and in the file `model_properties.txt` in the sub-directory `Models`

(2) The high precision of the solar data makes it very easy to use the ϵ method to determine which of the five models has the closest structure to the Sun. A simple visual inspection of ϵ differences between the Sun and the models is enough to show that models (3) has a large mismatch and that model (4) is bad too. The other three models are quite good, with models (1) and (5) being the best. Note that ϵ differences *must* be calculated at the observed frequencies for this to work.

Exercises for Chapter 9

(2) MHD and OPAL give difference results for the amplitude for the same helium abundance. More about this can be found in Basu et al., 2004, *Mon. Not. R. Astron. Soc.*, **350**, 277. In particular, see Fig. 8 of the paper.

(3) The true value of $\Delta\Pi_1$ for models RGB_ModelA, RGB_ModelB and RGB_ModelC are 77.4s, 29.08s and 263.9s respectively.